

Spin-dependent potentials for deuteron-nucleus scattering*

L. D. Knutson[†] and W. Haerberli

University of Wisconsin, Madison, Wisconsin 53706

(Received 7 July 1975)

Measurements of the cross section, the vector analyzing power, and the three tensor analyzing powers for deuteron elastic scattering from ^{90}Zr at 5.5 MeV and from ^{208}Pb at 9.0 MeV are presented. These measurements and additional measurements obtained from the literature are analyzed in terms of the optical model. The folding model is used to calculate the spin-dependent potentials from the known nucleon-nucleus potentials, and the central terms in the optical potential are determined empirically. Acceptable agreement is obtained for the cross section and vector analyzing power. The calculations reproduce the observed tensor analyzing powers for sub-Coulomb energies but not for energies above the Coulomb barrier.

NUCLEAR REACTIONS $^{90}\text{Zr}(\vec{d}, d)$, $E_d = 5.5$ MeV; $^{208}\text{Pb}(\vec{d}, d)$, $E_d = 9.0$ MeV; measured polarization parameters iT_{11} , T_{20} , T_{21} , $T_{22}(E_d, \theta)$; cross sections $\sigma(E_d, \theta)$. Enriched targets, optical model analysis.

I. INTRODUCTION

In this paper we present measurements of the cross section and analyzing powers¹ for deuteron elastic scattering from ^{90}Zr and ^{208}Pb at energies below the Coulomb barrier. These measurements, and additional measurements at higher energies obtained from the literature, are subjected to an optical model analysis in which the spin dependent terms in the potential are calculated from the folding model.² In this model, one assumes that the deuteron-nucleus potential is equal to the sum of the neutron-nucleus and proton-nucleus potentials averaged over the internal motion of the deuteron.

It has previously been shown that calculations using the folding model central potentials do not satisfactorily reproduce the measured differential cross sections.^{3,4} In order to obtain good agreement it is necessary to change the strength of the real central potential by 10–20% and to increase the strength of the imaginary potential.³ A 10–20% change in the strength of the central potential produces large changes in the calculated cross section and analyzing powers. Consequently, the usefulness of the folding model is limited. However, the model may still be useful to predict the spin dependent parts of the potential and thus to reduce ambiguities in the optical model analysis which result from the large number of parameters. Less accuracy is required for the spin dependent terms, since they are relatively weak compared to the central potential. Our purpose here is to determine whether the spin-orbit and tensor potentials predicted by the folding model are quantitatively consistent with the observed vector and tensor

analyzing powers for deuteron elastic scattering.

In Sec. II the experimental apparatus and the analyzing power measurements will be described. In Sec. III we will discuss the predicted spin dependence of the Coulomb part of the deuteron-nucleus potential. The calculation of the nuclear part of the potential will be described in Sec. IV. The optical model calculations will be presented in Secs. V and VI. Some of the results to be discussed here have previously been reported elsewhere.⁵

II. MEASUREMENTS

Angular distributions of the differential cross section, the vector analyzing power (iT_{11}), and the three tensor analyzing powers (T_{20} , T_{21} , and T_{22}) have been measured for deuteron elastic scattering from ^{90}Zr at 5.5 MeV and from ^{208}Pb at 9.0 MeV. The measurements were carried out using the deuteron beam from the University of Wisconsin Lamb-shift polarized ion source.⁶ The analyzing powers presented here are defined according to the Madison Convention⁷; a more detailed discussion of these quantities can be found in Ref. 1.

The measurements were carried out as follows. A beam of polarized deuterons was incident on a self-supporting target made from isotopically enriched material (98.1% for ^{90}Zr and 99.5% for ^{208}Pb). The targets were approximately 1 mg/cm² thick. Scattered deuterons and reaction products were detected by counter telescopes located to one side of the beam. Four telescopes were used to measure the analyzing powers at four angles simultaneously. The detected particles were identified by an on-line computer program⁸ which makes

use of the particle identification technique of Hird and Ollerhead.⁹ The measurements were corrected for the electronic dead time of the counting system using the technique described in Ref. 10. The fractional dead time was less than 1% in all cases.

Beam integration was accomplished by counting the number of deuterons scattered into two monitor detectors located symmetrically to the left and right of the beam at 13.1°. The counting rate for the monitor detectors is independent of the polarization state of the beam, since the analyzing powers are essentially zero at far forward angles according to optical model calculations. Thus, the ratio of the number of counts obtained for a detector telescope located at angle θ to the number of counts obtained for the monitor detectors is proportional to the polarized-beam cross section. This beam integration technique has the advantage that the ratio of counts is insensitive to nonuniformities in the target thickness.

The details of the procedure used to measure the vector¹¹ and tensor¹⁰ analyzing powers have previously been described in the literature. Using these methods, one obtains, in addition to the analyzing powers, a measure of the relative unpolarized cross section. Values of the absolute cross section were deduced under the assumption that the elastic scattering cross section at 13.1° is equal to the Rutherford cross section.

The measured differential cross sections have relative errors of 2% which result from uncertainties in the detector telescope solid angles and from uncertainties in extracting the number of counts from the pulse height spectrum. In addition, the absolute cross sections are subject to an over-all normalization error of 2% resulting from the uncertainty in the monitor detector solid angles. The major contribution to the uncertainty in the measured analyzing powers results from the statistical error in the measurements. Errors resulting from uncertainties in the beam polarization are negligible. Possible systematic errors resulting from shifts in the angle or position of the beam are estimated to be at least a factor of 2 smaller than the statistical errors. The errors shown in the figures are statistical only.

The analyzing powers were measured in angular steps of 5° for ²⁰⁸Pb and 6° for ⁹⁰Zr. The measurements and optical model calculations show that the analyzing powers change slowly with scattering angle and consequently the measurements provide many more data points than are necessary to determine the angular dependence of the analyzing powers. In order to reduce the size of the statistical errors, measurements obtained at three adjacent angles were statistically combined.

III. SPIN DEPENDENCE IN COULOMB SCATTERING

In this section we consider the elastic scattering of deuterons by a pure Coulomb field. It will be shown that the Coulomb potential energy contains a spin dependent term if the deuteron D state is taken into account. The analyzing powers which arise from this Coulomb interaction will be calculated and the results compared with the observed analyzing powers for sub-Coulomb scattering.

Consider the potential energy $V_c(\vec{r})$ of a deuteron whose c.m. is at position \vec{r} with respect to a point charge Ze . Since the Coulomb force acts only on the proton, the potential energy of the deuteron must be equal to the electrostatic potential evaluated at the position of the proton and averaged over the internal motion of the deuteron; i.e.,

$$\langle m | V_c(\vec{r}) | m' \rangle = \langle \phi_d^m | \frac{Ze^2}{|\vec{r} + \frac{1}{2}\vec{\rho}|} | \phi_d^{m'} \rangle, \quad (1)$$

where $\vec{\rho}$ is the neutron-proton separation and $|\phi_d^m\rangle$ is the internal wave function of a deuteron with magnetic quantum number m . It can be shown¹² that Eq. (1) reduces to

$$V_c(r) = Ze^2/r + \frac{3}{2}Q(Ze^2/r^3)T_r, \quad (2)$$

where Q is the deuteron quadrupole moment and where T_r is a tensor spin operator defined as

$$T_r = \frac{(\vec{s} \cdot \vec{r})^2}{r^2} - \frac{2}{3}. \quad (3)$$

In Eq. (3), the quantity \vec{s} is the deuteron spin operator. The term in Eq. (2) which contains Q will be referred to as the Coulomb tensor potential. The existence of the tensor potential which results from the Coulomb interaction was first noted by Raynal.¹³

There is a straightforward classical interpretation of the Coulomb tensor potential. The quadrupole moment is defined as the expectation value of $(3z^2 - r^2)$ in the state for which $m=j$ (i.e., the state for which \vec{s} lies along the z axis). The fact that the deuteron quadrupole moment is positive means that the deuteron charge density distribution is elongated along the direction of the deuteron spin axis. The Coulomb potential energy is obtained by averaging the electrostatic potential over this nonspherical charge distribution. Since the curvature (the second derivative with respect to r) of the electrostatic potential is positive, the overlap of the deuteron charge distribution with the electrostatic potential is greater for \vec{s} parallel (or antiparallel) to \vec{r} than for \vec{s} perpendicular to \vec{r} . This corresponds to the result that the Coulomb tensor potential is positive for \vec{s} parallel to \vec{r} and negative for \vec{s} perpendicular to \vec{r} . The radial dependence of the Coulomb tensor potential, r^{-3} , is proportional

to the second derivative of the electrostatic potential, as one would expect from the above discussion.

The effect of the Coulomb tensor potential on the analyzing powers for elastic scattering is small because the potential is weak. Using the measured value of the deuteron quadrupole moment,¹⁴ we find that the tensor potential is only 0.4% of the central Coulomb potential at a radius of 10 fm. Although the tensor potential is weak, it extends to rather large radii since it falls off as r^{-3} , whereas the nuclear forces fall off exponentially outside the nucleus. Thus, for energies sufficiently far below the Coulomb barrier, the analyzing powers for deuteron elastic scattering should arise primarily from the Coulomb potential.

The effect of the Coulomb tensor potential on the deuteron scattering process was calculated using the distorted-wave Born approximation for elastic scattering. The method employed is similar to a method developed by Kim and Thomas.¹⁵ The distorting potential was taken to be Ze^2/r , so that the distorted waves are just the Coulomb wave functions. The Coulomb tensor potential was treated as a perturbation. When this approximation is used one obtains a closed form expression for the cross section and the analyzing powers. The details of this calculation can be found in Ref. 12. The calculated values of iT_{11} and T_{20} for ^{208}Pb at 9 MeV are compared with the measurements in Fig. 1. One notes that for T_{20} the calculations are roughly a factor of 2 or 3 smaller in magnitude than the measurements, although the sign and shape of the analyzing powers are correctly predicted. Similar results were obtained for T_{21} and T_{22} . The disagreement between the calculations and the measurements is even more pronounced for iT_{11} . The magnitude of the measured vector analyzing power is typically 0.005, whereas the calculated values are zero. It appears that the nuclear spin dependent forces have a significant influence on the measurements.

IV. FOLDING MODEL POTENTIALS

In this section we discuss the nuclear spin dependent potentials predicted by the folding model. In this model the deuteron-nucleus potential is given by²

$$\langle m | V(\vec{r}) | m' \rangle = \langle \phi_d^m | [V_n(\vec{r} - \frac{1}{2}\vec{p}) + V_p(\vec{r} + \frac{1}{2}\vec{p})] | \phi_d^{m'} \rangle, \quad (4)$$

where V_n and V_p are the neutron-nucleus and proton-nucleus potentials, respectively. If the nucleon-nucleus potentials in Eq. (4) consist of central and spin-orbit terms, the deuteron potential will likewise contain a central and a spin-orbit term.² If the deuteron D state is included in the

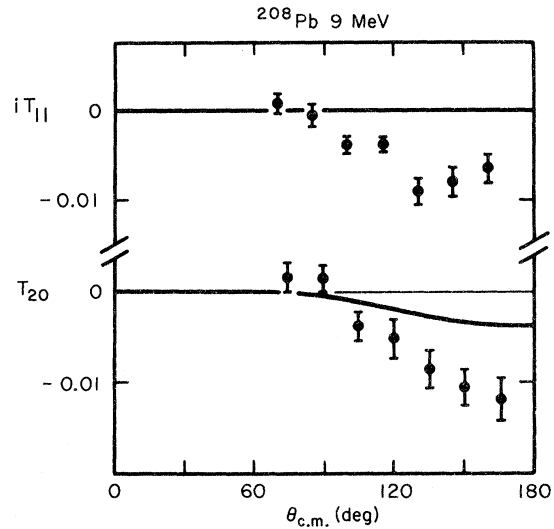


FIG. 1. Angular distributions of the analyzing powers iT_{11} and T_{20} for deuteron elastic scattering from ^{208}Pb at 9 MeV. The curves show the calculated analyzing powers for the potential given in Eq. (2), which includes Coulomb interactions only. The calculated values of iT_{11} are zero.

calculation, the deuteron potential will in addition contain a tensor potential of the form¹⁶

$$V_T(\vec{r}) = F(r)T_r, \quad (5)$$

where T_r is defined in Eq. (3).

The folding model potentials were calculated from Eq. (4) using the method of Raynal.¹³ The potentials V_n and V_p were obtained from the analysis of Becchetti and Greenlees,¹⁷ and the deuteron wave function was taken to be that derived from the nucleon-nucleon potential of Hamada and Johnston.¹⁸

The calculated spin dependent potentials for ^{90}Zr are shown in Fig. 2. The tensor potential is complex because the nucleon-nucleus central potential, from which it arises, is complex. The folding model spin-orbit potential is purely real since it arises from the nucleon-nucleus spin-orbit potentials which are assumed to be real at these energies. The potentials for ^{208}Pb are similar, but are slightly smaller in magnitude and extend to a larger radius than the ^{90}Zr potentials.

A. Tensor potential

As discussed in Sec. III, the tensor potential arises because the deuteron is not spherically symmetric. The real part of the tensor potential shown in Fig. 2 has a qualitative resemblance to the second derivative of the nucleon-nucleus central potential (see

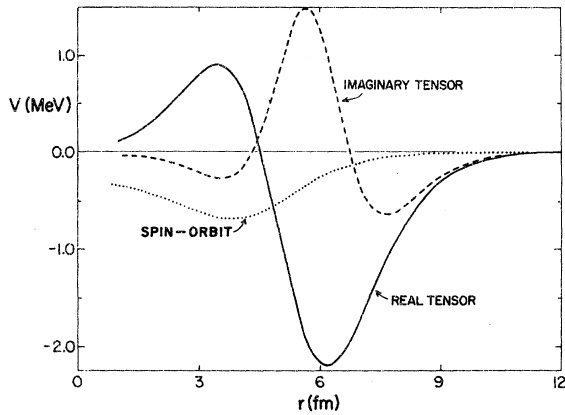


FIG. 2. Spin dependent parts of the folding model potential for ^{90}Zr as a function of the deuteron-nucleus separation. The real and imaginary parts of $F(r)$ [see Eq. (5)] are given by the solid and dashed curves, respectively. The spin-orbit potential is obtained by multiplying the dotted curve by $\vec{l} \cdot \vec{s}$.

Ref. 4) as one would expect from the argument in Sec. III. The tensor potential is largest in magnitude in the region of the nuclear surface where the curvature of the nucleon-nucleus central potential is greatest.

There is little available phenomenological information concerning the nature of the tensor potentials in the deuteron-nucleus interaction, because there have been few tensor analyzing power measurements until recently and because the optical model analyses of these measurements have not been very successful. Several authors¹⁹⁻²⁴ have shown that the addition of tensor terms in the optical model potential improves the agreement with measured tensor analyzing powers. However, these analyses have not been sufficiently extensive to allow a quantitative determination of the tensor potential.

B. Spin-orbit potential

The spin-orbit (so) potential predicted by the folding model can be reproduced quite accurately by an analytic expression of the form normally used in optical model calculations⁴,

$$V_{so}(r) = V_{so} \left(\frac{\hbar}{m_{\pi}c} \right)^2 \frac{1}{a_{so}} \frac{1}{r} e^x (1+e^x)^{-2} \vec{l} \cdot \vec{s}, \quad (6)$$

where

$$x = (r - r_{so} A^{1/3}) / a_{so}. \quad (7)$$

The constant $(\hbar/m_{\pi}c)^2$ in Eq. (6) has the numerical value 2.0 fm^2 . The values of the parameters V_{so} , r_{so} , and a_{so} for which Eq. (6) most accurately repro-

duces the folding model potential are listed in Table I. In Fig. 3, the exact folding model potential for ^{90}Zr (solid curve) is compared with the potential calculated from Eq. (6) using the parameters listed in Table I (dotted curve). It would appear that for most purposes the exact potential and the analytic representation can be used interchangeably.

It is interesting to compare the folding model spin-orbit potential with the spin-orbit potentials which have been used in previous phenomenological optical model analyses (see, for example, Ref. 25 and references cited therein). Typical values of the parameters which describe the phenomenological spin-orbit potential are

$$V_{so} = 7 \text{ MeV}, \quad r_{so} = 0.8 \text{ fm}, \quad a_{so} = 0.5 \text{ fm}. \quad (8)$$

The primary difference between the potential given in Eq. (8) and those listed in Table I is that the diffuseness parameter is larger for the folding model potential. Note that the analytic expression for the spin-orbit potential contains a factor $1/a_{so}$, and consequently the folding model potential is smaller in magnitude at its peak than the phenomenological potential. In Fig. 3 we compare the spin-orbit potential predicted by the folding model with the phenomenological potential defined by Eq. (8) (dashed curve). This comparison shows that the phenomenological potential is significantly deeper and more sharply peaked than the folding model potential.

Spin-orbit parameters similar to those given in Eq. (8) have consistently been used in optical model calculations in the past. However, it is well known that the quality of fits to vector analyzing power measurements is quite insensitive to the values of a_{so} and r_{so} (see Refs. 26 and 27). For example, Brown *et al.*²⁵ have shown that one can obtain reasonable fits to measurements of the vector analyzing power using values of a_{so} as small as 0.18 fm. Thus, we can not exclude the possibility that the correct value of a_{so} is, in fact, near 1 fm.

TABLE I. Spin-orbit parameters predicted by the folding model.

Target	V_{so} (MeV)	r_{so} (fm)	a_{so} (fm)
^{48}Ti	5.35	0.98	0.97
^{63}Zn	5.54	0.97	0.99
^{90}Zr	5.63	0.98	1.00
^{120}Sn	5.69	0.98	1.00
^{208}Pb	5.79	0.99	1.01

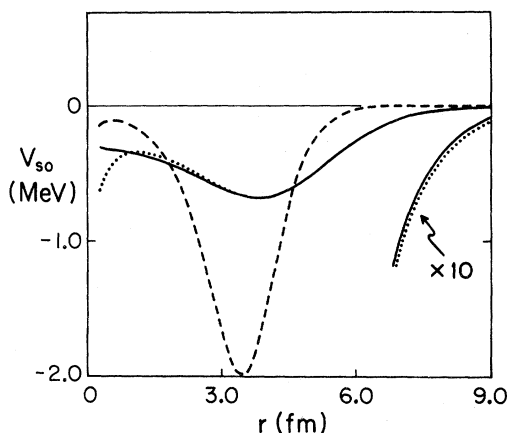


FIG. 3. Spin-orbit potentials for ^{90}Zr as a function of the deuteron-nucleus separation. The solid curve is the potential predicted by the folding model. The dotted curve shows the analytic potential [Eq. (6) and the parameter values in Table I] which closely approximates the folding model potential. The dashed curve shows a typical phenomenological potential which is defined by the parameters in Eq. (8).

V. ANALYSIS OF THE VECTOR ANALYZING POWER MEASUREMENTS

In this section we will describe the optical model analysis of measured cross sections and vector analyzing powers for deuteron elastic scattering from several target nuclei. The measurements, which were obtained from the literature, are for deuteron scattering from ^{48}Ti and ^{68}Zn at 9 MeV (Ref. 28), from ^{90}Zr at 10 MeV (Ref. 29), from ^{120}Sn at 11 MeV (Ref. 28), and from ^{208}Pb at 12.3 MeV (Ref. 30).

The nuclear central potential used in the analysis was expressed in the usual way. The real central potential was a Woods-Saxon well with depth V , radius $r_0 A^{1/3}$, and diffuseness a_0 . The imaginary potential was a surface-peaked derivative Woods-Saxon well of depth W , radius $r_I A^{1/3}$, and diffuseness a_I . The Coulomb potential was taken to be that of a uniformly charged sphere of radius $1.3A^{1/3}$ fm.

The spin-orbit potentials used in the analysis were taken directly from the folding model. With the exception of ^{208}Pb , the potentials used were the parametrized expressions which closely approximate the folding model predictions. For ^{208}Pb the exact folding model potential did not agree accurately with Eq. (6) at large r . For this case the exact potential was used. Tensor potentials were not included in the calculations since these quantities have little effect on the vector analyzing

power (see Sec. VI).

The six parameters describing the nuclear central potentials were adjusted to obtain a good fit to the measured cross sections and vector analyzing powers. The final parameters are listed in Table II, and the measurements and optical model predictions (solid curves) are shown in Fig. 4. Although there are some systematic disagreements between the calculations and the measurements, the over-all quality of the fits is similar to that obtained in standard optical model calculations in which the spin-orbit potential is treated phenomenologically. To illustrate this point, the optical model analysis for three of the target nuclei was

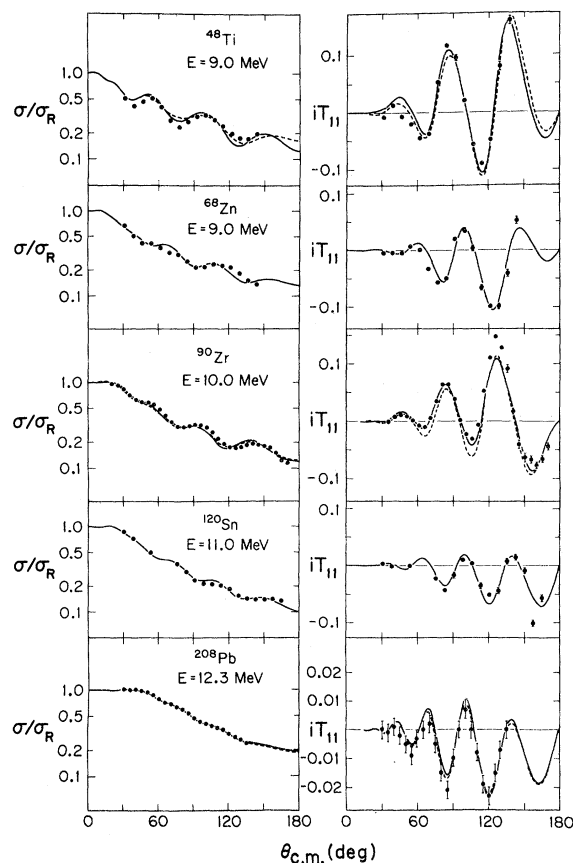


FIG. 4. Angular distributions of the differential cross section and the vector analyzing power for deuteron elastic scattering from a variety of target nuclei. The measurements are from Refs. 28–30. The cross sections are given as ratios to the Rutherford cross section. The solid curves are the result of optical model calculations which make use of the folding model spin-orbit potential. The dashed curves were obtained in the same manner as the solid curves, except that the spin-orbit potential defined in Eq. (8) was used. For ^{208}Pb the solid and dashed curves are virtually identical.

TABLE II. Optical model parameters determined by fitting the cross section and vector analyzing power measurements. The column labeled "spin-orbit" indicates whether the spin-orbit potential was that predicted by the folding model (FM) or the typical phenomenological potential which is defined in Eq. (8).

Target	Energy (MeV)	V (MeV)	r_0 (fm)	a_0 (fm)	W (MeV)	r_I (fm)	a_I (fm)	Spin-orbit
^{48}Ti	9.0	88.0	1.20	0.58	7.83	1.48	0.93	FM
^{68}Zn	9.0	100.5	1.15	0.56	5.69	1.85	0.93	FM
^{90}Zr	10.0	104.0	1.10	0.91	12.48	1.48	0.67	FM
^{120}Sn	11.0	115.3	1.05	0.75	6.33	1.68	0.87	FM
^{208}Pb	12.3	120.4	1.05	0.83	5.35	1.52	0.91	FM
^{48}Ti	9.0	96.6	1.10	0.65	8.08	1.55	0.92	Eq. (8)
^{90}Zr	10.0	106.6	1.05	0.97	10.85	1.57	0.71	Eq. (8)
^{208}Pb	12.3	122.5	1.05	0.76	4.76	1.54	0.95	Eq. (8)
^{90}Zr	5.5	94.8	1.20	0.58	6.54	1.77	0.72	FM
^{208}Pb	9.0	130.2	1.05	0.72	2.45	1.67	0.88	FM

repeated using the spin-orbit potential defined by Eq. (8). The parameters obtained in this analysis are given in Table II and the resulting calculations are shown by the dashed curves in Fig. 4. The change from the folding model potential to the more standard spin-orbit potential did not improve the agreement with the measurements.

VI. ANALYSIS OF THE TENSOR ANALYZING POWER MEASUREMENTS

We now include the folding model tensor potentials in the optical model calculations. The tensor

potentials primarily affect the calculated tensor analyzing powers and have little influence on the cross section and vector analyzing power. Measurements of the tensor analyzing powers for deuteron scattering from ^{90}Zr at 10 MeV (which have been provided by Goddard²⁹) are shown in Fig. 5. The solid curves in the figure are the result of the optical model calculation described in the preceding section. The potential used in this calculation contains no tensor term and thus the predicted tensor analyzing powers are small in magnitude.

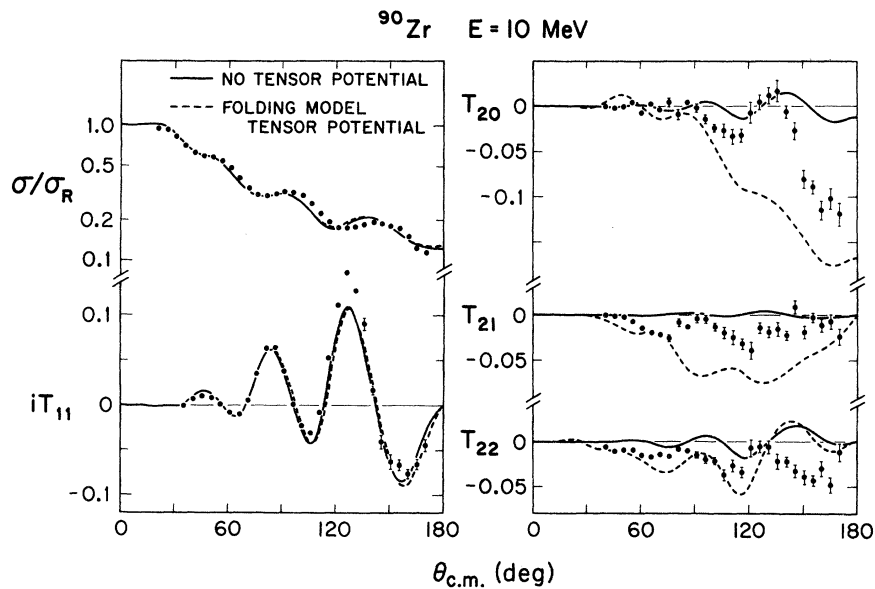


FIG. 5. Angular distributions of the differential cross section and the four analyzing powers for deuteron elastic scattering from ^{90}Zr at 10 MeV. The measurements are from Ref. 29. The cross sections are given as ratios to the Rutherford cross section. The solid curves show the result of an optical model calculation using a potential which contains no tensor term. The dashed curves show the predictions which one obtains when the folding model tensor potential is included.

The dashed curves in Fig. 5 show the analyzing powers which result when the folding model tensor terms are included in the potential and the analyzing powers are simply calculated without further adjustment of the parameters. The agreement of this calculation with the measured tensor analyzing powers is poor. The trend of the calculation is generally in the right direction (i.e., the addition of the tensor potential results in tensor analyzing powers which are larger in magnitude and predominantly negative), but the calculated analyzing powers are too large in magnitude. In addition, the calculation fails to reproduce the oscillations in the measurements.

Calculations of the type shown in Fig. 5 have been carried out for several medium weight nuclei by Goddard and Haeberli.³¹ For deuteron energies above the Coulomb barrier, these calculations consistently fail to reproduce the measured tensor analyzing powers.

The failure of the optical model calculations to reproduce the measured tensor analyzing powers does not necessarily mean that the tensor potentials predicted by the folding model are incorrect. Since the calculated tensor analyzing powers are substantial in magnitude even in the absence of tensor potentials, it is possible that the poor agreement results from the use of inaccurate central or spin-orbit potentials. For sub-Coulomb energies the calculated tensor analyzing powers should be less sensitive to errors in the central and spin-orbit potentials.

The measurements and optical model calculations for sub-Coulomb scattering from ^{90}Zr and ^{208}Pb are shown in Fig. 6. As in the analysis described in Sec. V, the central potentials were determined by fitting the cross section and vector analyzing power measurements, using a potential which contained the folding model spin-orbit term and no tensor term. The final parameter values for the two nuclei are given in Table II, and the fits are shown by the solid curves in Fig. 6. The tensor analyzing powers predicted by this optical model calculation are much smaller in magnitude than the measurements.

By using perturbation theory, one can understand why the tensor analyzing powers are small. If the spin-orbit potential is treated as a perturbation, the resulting vector analyzing power is first order in the strength of the spin-orbit interaction, whereas the effect of the potential on the tensor analyzing powers is second order.³² For sub-Coulomb scattering the second-order effects should be much smaller in magnitude than the first-order effects. Consequently, if no tensor potentials are included, the calculated tensor analyzing powers must be small compared to the vector analyzing

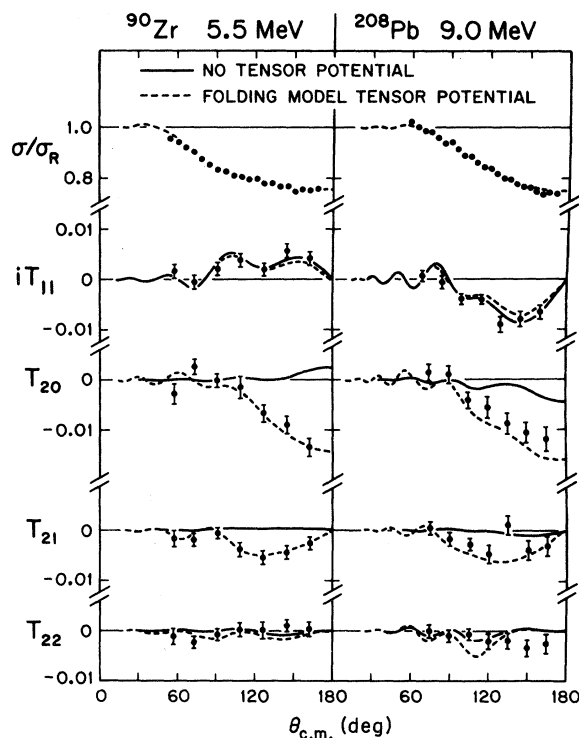


FIG. 6. Angular distributions of the differential cross section and the four analyzing powers for deuteron elastic scattering from ^{90}Zr at 5.5 MeV and from ^{208}Pb at 9 MeV. The cross sections are given as ratios to the Rutherford cross section. The solid curves show the result of optical model calculations using potentials which contain no tensor term. The dashed curves show the predictions which one obtains when the folding model tensor potential is included. For the differential cross sections, the solid and dashed curves are virtually identical.

power, regardless of the particular spin-orbit potential used. Because the measured vector and tensor analyzing powers are comparable in magnitude, it is concluded that a tensor term must be present in the potential.

The dashed curves in Fig. 6 show the cross section and analyzing powers which are predicted when the folding model tensor potentials are included in the optical model calculation. The agreement of these calculations with the measured tensor analyzing powers is satisfactory for both targets and is particularly good for ^{90}Zr .

The sub-Coulomb measurements discussed here do not provide a particularly stringent test of the folding model, since the analyzing powers are small in magnitude and show little structure. However, it is significant that the folding model tensor potentials successfully predicted the correct sign

and approximate magnitude of all three tensor analyzing powers for both target nuclei without the use of adjustable parameters.

VII. SUMMARY AND CONCLUSIONS

For the targets and energies considered here, the optical model calculations which make use of the folding model spin-orbit potential provide reasonable agreement with measurements of the vector analyzing power. For energies above the Coulomb barrier, the fits are comparable in quality to those obtained in calculations which use more standard spin-orbit potentials. We conclude that the measurements discussed here show no clear preference for either the folding model potential or for the standard phenomenological potential. In future analyses, it would be interesting to compare the two spin-orbit potentials over a wider range of targets and energies. If it should turn out that the two potentials consistently provide comparable fits, one would naturally prefer the folding model potential, since it is derived from a physical model of the interaction whereas the standard spin-orbit

potential has no simple physical basis.

When the folding model tensor potential was included in the analysis, the resulting optical model calculations successfully reproduced the measured tensor analyzing powers for sub-Coulomb scattering. However, a similar calculation for deuteron scattering from ^{90}Zr at 10 MeV was unsuccessful. In view of the mixed success of these results, it is not possible to draw firm conclusions concerning the accuracy of the folding model tensor potentials. The lack of agreement in the latter analysis is not necessarily the result of using an incorrect tensor potential, but could also result from the use of inaccurate central potentials. Alternatively, the deterioration of the fits with increasing energy may be an indication that the folding model potential is correct outside the nucleus but inaccurate in the nuclear interior. The resolution of these questions will require more detailed optical model analyses.

The authors are indebted to J. M. Lohr and R. P. Goddard for allowing us to make use of their analyzing power measurements prior to publication.

*Work supported in part by the U. S. Atomic Energy Commission.

†Present address: Nuclear Physics Laboratory, University of Washington, Seattle, Washington 98195.

¹S. E. Darden, in *Polarization Phenomena in Nuclear Reactions*, edited by H. H. Barschall and W. Haerberli (Univ. of Wisconsin Press, Madison, 1971), p. 39.

²S. Watanabe, Nucl. Phys. **8**, 484 (1958).

³F. G. Perey and G. R. Satchler, Nucl. Phys. **A97**, 515 (1967).

⁴P. W. Keaton, Jr., and D. D. Armstrong, Phys. Rev. **C 8**, 1692 (1973).

⁵L. D. Knutson and W. Haerberli, Phys. Rev. Lett. **30**, 986 (1973).

⁶T. B. Clegg, G. A. Bissinger, W. Haerberli, and P. A. Quin, in *Polarization Phenomena in Nuclear Reactions* (see Ref. 1), p. 835.

⁷*Polarization Phenomena in Nuclear Reactions* (see Ref. 1), p. xxv.

⁸S. E. Vigdor and H. Liers, University of Wisconsin Internal Report OPIS71, 1971 (unpublished).

⁹B. Hird and R. W. Ollerhead, Nucl. Instrum. Methods **71**, 231 (1969).

¹⁰N. Rohrig and W. Haerberli, Nucl. Phys. **A206**, 225 (1973).

¹¹D. C. Kocher and W. Haerberli, Nucl. Phys. **A172**, 652 (1971).

¹²L. D. Knutson, Ph.D. thesis, University of Wisconsin, 1973 (available from University Microfilms, Ann Arbor, Michigan).

¹³J. Raynal, Ph.D. thesis, Commissariat à l'énergie Atomique, Centre d'Études Nucleaires de Saclay Report No. CEA-R-2511, 1965 [Argonne National Labora-

tory Report No. ANL-TRANS-258, 1965 (unpublished)].

¹⁴R. V. Reid, Jr., and M. L. Vaida, Phys. Rev. Lett. **29**, 494 (1972).

¹⁵Y. N. Kim and H. C. Thomas, Phys. Rev. **148**, 1083 (1966).

¹⁶G. R. Satchler, Nucl. Phys. **21**, 116 (1960).

¹⁷F. D. Becchetti, Jr., and G. W. Greenlees, Phys. Rev. **182**, 1190 (1969).

¹⁸T. Hamada and I. D. Johnston, Nucl. Phys. **34**, 382 (1962).

¹⁹P. Schwandt and W. Haerberli, Nucl. Phys. **A123**, 401 (1969).

²⁰A. Djaloeis and J. Nurzynski, Nucl. Phys. **A163**, 113 (1971).

²¹A. Djaloeis and J. Nurzynski, Nucl. Phys. **A181**, 280 (1972).

²²G. Perrin *et al.*, Nucl. Phys. **A206**, 623 (1973).

²³M. Irshad and B. A. Robson, Nucl. Phys. **A218**, 504 (1974).

²⁴R. Roche, N. VanSen, G. Perrin, J. C. Gondrand, A. Fiore, and H. Müller, Nucl. Phys. **A220**, 381 (1974).

²⁵R. C. Brown, A. A. Debenham, J. A. R. Griffith, O. Karban, D. C. Kocher, and S. Roman, Nucl. Phys. **A208**, 589 (1973).

²⁶P. Schwandt and W. Haerberli, Nucl. Phys. **A110**, 585 (1968).

²⁷J. A. R. Griffith, M. Irshad, O. Karban, and S. Roman, Nucl. Phys. **A146**, 193 (1970); *ibid.* **A166**, 675(E) (1971).

²⁸J. M. Lohr, Ph.D. thesis, University of Wisconsin, 1972 (available from University Microfilms, Ann Arbor, Michigan).

²⁹R. P. Goddard (private communication).

³⁰S. E. Vigdor, R. D. Rathmell, H. S. Liers, and
W. Haeberli, Nucl. Phys. A210, 70 (1973).

³¹R. P. Goddard and W. Haeberli, Bull. Am. Phys. Soc.

18, 1393 (1973).

³²D. J. Hooten and R. C. Johnson, Nucl. Phys. A175,
583 (1971).